Gaussian Orbital Determination of 1685 Toro - 1948 OA

THE PHOENIXES (TEAM 11)
Crystal Luo, Tiffany Pan, Sean Jung
Summer Science Program 2015

I. INTRODUCTION

THE purpose of the experiment was to determine the orbit of the near-earth asteroid 1685 Toro (1948 OA) from CCD images of the asteroid taken during June and July 2015. Observations were conducted with a 14" Celestron Schmidt Cassegrain telescope at Etscorn Observatory in New Mexico Tech in Socorro, NM and a 20" Ritchey Chretien telescope located at the Calumet Astronomy Center at Purdue University in Lowell, Indiana. The orbital elements were determined using Gauss' method of orbital determination.

It is vitally important to analyze the orbit of Toro since it intersects the Earth's orbit and numerical integration techniques can reveal whether a collision with the Earth is likely. However improbable a collision with Toro may be, orbital determination remains essential since the solar system is littered with potential impacters. Finally, the orbital elements of Toro and similar asteroids are necessary when considering future missions to asteroids for analysis or retrieval.

II. MATERIALS AND METHODS

The images were taken using two telescopes, one located in Socorro, New Mexico (253° 05' 09.9" E, 34° 04' 21.6" N) and one in Calumet, Indiana (272° 37' 28.9" E, 41° 16' 15.0" S).

TABLE I: *Telescopes Used for Data Collection*

Telescope Type	Diameter	Location
Celestron Schmidt-Cassegrain	0.36-m	Socorro. NM
Ritchey-Chretien	0.51-m	Lowell, IN

In addition to the two telescopes used to collect data, computer software assisted in the data collection and analysis processes. The various software used include CCDSoft Version 5, TheSky6, TheSkyX Pro, and STCF-5 Focuser.

I. Data Collection

A. Etscorn Observations: Before each scheduled observation, the location of 1685 Toro was estimated by obtaining ephemerides generated using the JPL Horizons database. TheSkyX Pro was used to generate a star finder chart that aided in predicting Toro's position with reference to other stars in the field of view and helped confirm that the telescope was slewed to the correct position by matching stars in the resulting CCD image with corresponding stars in the SkyX field.

The first usable set of images, in which the asteroid was identified, was taken between 5:00 and 7:00 UTC. All subsequent observations at Etscorn took place between 3:00 and 5:00 UTC. At the start of each observation, the CCD chip was cooled to -10°C. The asteroid was located by focusing the telescope to various pointing stars with magnitude of approximately 10 V, and then slewing to the asteroid's predicted equatorial coordinates. After focusing the telescope through taking a series of test images, multiple sets of 5 images with 2x2 binning and 45 or 60 second exposures were taken with a waiting period of 15 - 20 minutes. Multiple sets over time were taken so the asteroid's movement relative to the stars would reveal its location in the image.

During each observation, 11 bias frames, 5 dark frames, and 11 flat field images were taken for image reduction purposes. Biases had 0 exposure time and required a closed shutter, darks had finite exposure time (usually 45 or 60 seconds) with a closed shutter, and flats also had a finite exposure time of usually 45 or 60 seconds with an open shutter.

B. Calumet Observations: Whenever a scheduled observation was cancelled due to the weather at Etscorn Observatory, we would defer to the 2-" Ritchey-Chretien telescope located at the Calumet Astronomy center at Purdue University in Lowell, Indiana. The telescope itself was remotely operated by Dr. Adam W. Rengstorf from his laptop in Socorro. An ephemeris for 1948 OA at the specified time and location was generated and used to guide the telescope in taking 5 sets of 5 60 second exposures with 5 min. between each set. When all the images were successfully taken, Dr. Rengstorf provided us with an online link containing folders with our FITS files.

II. Observations

The following is a list of observations and details from each night of observing:

6/26/15 5:00-7:00 UTC
Predicted position (α, δ) : ($15^h53^m08.2^s$, -25°30'43.6")
Telescope: 14" Celestron Schmidt-Cassegrain
Filter: Visual
Exposure Time: 10 sec. test, 75 second images
Number of Images: 9
Quality of Images: Bad quality due to clouds, filled with noise

6/28/15 5:00-7:00 UTC
Predicted position (α, δ) : ($15^h49^m41.8^s$, -25°01'03.1")
Cancelled due to weather

7/2/15 3:00-5:00 UTC
Predicted position (α, δ) : ($15^h43^m39.1^s$, -24°03'44.6")
Telescope: 14" Celestron Schmidt-Cassegrain
Filter: Visual
Exposure Time: 10 sec. test, 45 second images
Number of Images: 15
Quality of Images: One usable set, one clouded out, one streaked

7/9/15 3:00-5:00 UTC
Predicted position (α, δ) : ($15^h35^m12.54^s$, -22°26'53.3")
Telescope: 14" Celestron Schmidt-Cassegrain
Filter: Visual
Clouded out, performed Cloudy Night Experiment
Number of Images: 5 sets of darks (5 images) and biases (11 images) at varied exposure times, 11 sets of darks (5 images) and 10 sets of biases (11 images) at varied temperatures [Note: we did not finish the last set of biases]

7/13/15 3:00-5:00 UTC
Predicted position (α, δ) : ($15^h31^m46.8^s$, -21°36'15.1")
Telescope: 14" Celestron Schmidt-Cassegrain
Filter: Visual
Exposure Time: 1 sec and 15 sec tests
Number of Images: 1 and the last set of 11 bias images for the Cloudy Night Data
Quality of Images: Out of focus and unusable

7/15/15 2:00-4:00 UTC
Predicted position (α, δ) : ($15^h31^m07.4^s$, -21°24'59.0")
Telescope: 20" Ritchey-Chretien
Filter: Visual
Exposure Time: 60 sec
Number of Images: 20 images
Quality of Images: good quality, asteroid identifiable

7/17/15 3:00-5:00 UTC
Predicted position (α, δ) : ($15^h29^m21.34^s$, -20°49'46.7")
Clouded out

7/19/15 3:00-5:00 UTC
Predicted position (α, δ) : ($15^h28^m30.67^s$, -20°28'12.4")
Cancelled due to weather

7/20/15 2:00-3:00 UTC
Predicted position (α, δ) : ($15^h28^m11.90^s$, -20°18'29.9")
Telescope: 20" Ritchey-Chretien
Filter: Visual
Exposure Time: 60 second images
Number of Images: 5 x set of 5: 5 min. between (25 tot)
Quality of Images: good quality

7/21/15 3:00-5:00 UTC
Predicted position (α, δ) : ($15^h27^m54.27^s$, -20°07'46.3")
Telescope: 14" Celestron Schmidt-Cassegrain
Filter: Visual
Exposure Time: 60 second images
Number of Images: 2 sets of 5 images; 15 min. between
Quality of Images: good quality, asteroid identified

III. Image Processing

Each set of images taken during observations were reduced using median-combined biases, average darks, and average flats. In order to locate the asteroid, the reduced images were then aligned and blinked through using CCDSoft. We could discern our asteroid as the surrounding stars remained stationary while our asteroid moved in its orbit through the blinked set of images.

IV. Image Measuring

Reference stars were identified in the images by comparing the stars in each image to the corresponding star field in the astronomy software TheSkyX. 24 reference stars were identified around the asteroid and used to optimize the balance between precision and efficiency. After recording the equatorial coordinates and centroids, the x and y coordinates of each star's center weighted by intensity pixel count, a least squares plate reduction was used to calculate the best linear regression that mapped each (x, y) pixel location to a right ascension and declination. The regression is calculated in the following form:

$$\alpha = b_1 + a_{11}x + a_{12}y, \tag{1}$$

$$\delta = b_2 + a_{21}x + a_{22}y. \tag{2}$$

A Python program was written to calculate the plate constants (the coefficients) by solving the following matrices:

$$\begin{pmatrix} \sum \alpha_i \\ \sum \alpha_i x_i \\ \sum \alpha_i y_i \end{pmatrix} = \begin{pmatrix} N & \sum x_i & \sum y_i \\ \sum x_i & \sum x_i^2 & \sum x_i y_i \\ \sum y_i & \sum x_i y_i & \sum y_i^2 \end{pmatrix} \cdot \begin{pmatrix} b_1 \\ a_{11} \\ a_{12} \end{pmatrix},$$

$$\begin{pmatrix} \sum \delta_i \\ \sum \delta_i x_i \\ \sum \delta_i y_i \end{pmatrix} = \begin{pmatrix} N & \sum x_i & \sum y_i \\ \sum x_i & \sum x_i^2 & \sum x_i y_i \\ \sum y_i & \sum x_i y_i & \sum y_i^2 \end{pmatrix} \cdot \begin{pmatrix} b_2 \\ a_{21} \\ a_{22} \end{pmatrix}$$

for b_1, a_{11}, a_{12}, b_2, a_{21}, and a_{22}.

Through using a python program to measure the centroid location (c_{x_i}, c_{y_i}) of the asteroid in each image, the right ascension and declination (α_i, δ_i) at each observation were calculated using the regression equation. In addition, since the regression was imperfect, our uncertainty was determined by calculating the residual of each right ascension and declination coordinate, and taking the standard deviation of the residual values:

$$\sigma_\alpha = \sqrt{\frac{\sum_{i=0}^{n} (\hat{\alpha_i} - \alpha_i)^2}{n-3}}, \qquad \sigma_\delta = \sqrt{\frac{\sum_{i=0}^{n} (\hat{\delta_i} - \delta_i)^2}{n-3}}. \quad (3)$$

This process was applied to the three best sets of images to obtain a right ascension and declination input for the method of Gauss, which requires $(\alpha_1, \delta_1, t_1)$, $(\alpha_2, \delta_2, t_2)$, and $(\alpha_3, \delta_3, t_3)$, the equatorial angular coordinates of the asteroid at the three observation times.

V. Gaussian Orbital Determination

The method of Gauss, an iterative process with the implementation of calculus, was performed in Python to obtain the properties of $(\vec{r}, \dot{\vec{r}}, t)$ for the asteroid at the middle observation time. Once the position and velocity of the asteroid at a light-corrected observation time were obtained, the classical orbital elements and projected orbital model of 1685 Toro were determined using numerical integration.

Before we get into the actual calculations, we must define a couple variables. First, we must understand that units of time are based on:

$$\frac{a^3}{T^2} = GM = \mu \rightsquigarrow a^3 = (\sqrt{\mu} T)^2 \quad (4)$$

While observations yield $(t_1, \hat{\rho}_1)$, $(t_2, \hat{\rho}_2)$, and $(t_3, \hat{\rho}_3)$. For each observation, we define:

$$\vec{\rho}_i = \vec{R}_i + \vec{r}_i \quad (5)$$

Then, we define $\tau_1 = \mu(t_1 - t_2)$, $\tau_2 = \mu(t_3 - t_1)$, and $\tau_3 = \mu(t_3 - t_2)$. Finally, we define the constants a_1 and a_3 by the equation:

$$\vec{r}_2 = a_1 \vec{r}_{11} + a_3 \vec{r}_3 \quad (6)$$

We can make an initial estimate for a_1 and a_3, where $a_1 = \frac{\tau_3}{\tau_0}$ and $a_3 = -\frac{\tau_1}{\tau_0}$. From here, we can move on to preiteration.

For preiteration, the basic idea is that we use the initial estimates for a_1 and a_3 to find the estimates for the asteroid distances ρ_1, ρ_2, and ρ_3, then estimate the velocity of the asteroid at an initial time t_0. In order to do this, the first step is to solve the equation:

$$\vec{\rho}_2 = \vec{R}_2 + a_1(\vec{\rho}_1 - \vec{R}_1) + a_3(\vec{\rho}_3 - \vec{R}_3) \quad (7)$$

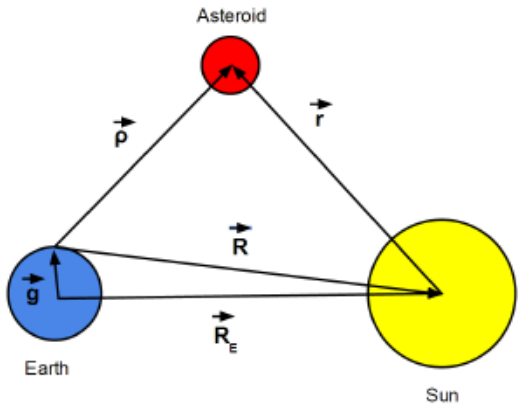

Fig. 1: *Diagram demonstrating relationship between relative positional vectors $\vec{\rho}, \vec{R_E}, \vec{R}, \vec{g}$, and $\vec{r}$.*

With ρ_1, ρ_2, and ρ_3, we can estimate the heliocentric vectors with the following expressions:

$$\vec{r}_1 = \rho_1 \hat{\rho}_1 - \vec{R}_1 \quad (8)$$

$$\vec{r}_2 = \rho_2 \hat{\rho}_2 - \vec{R}_2 \quad (9)$$

$$\vec{r}_3 = \rho_3 \hat{\rho}_3 - \vec{R}_3 \quad (10)$$

We can then estimate the velocity of the asteroid at t_0 by:

$$\dot{\vec{r}}_2 = \frac{1}{2}\left[\frac{\vec{r}_2 - \vec{r}_1}{-\tau_1} + \frac{\vec{r}_3 - \vec{r}_2}{-\tau_3}\right] \quad (11)$$

Now we write the orbit $\vec{r}(\tau)$ in terms of the basis $\{\vec{r}_2, \dot{\vec{r}}_2\} : \vec{r}(\tau) = f(\tau)\vec{r}_2 + g(\tau)\dot{\vec{r}}_2$. Here, $\tau = \sqrt{\mu}(t - t_2)$.

We now move on to the actual iteration, where we will develop more accurate values of the basis $\{\vec{r}_2, \dot{\vec{r}}_2\} : \vec{r}(\tau) = f(\tau)\vec{r}_2 + g(\tau)\dot{\vec{r}}_2$. The Taylor series of $\vec{r}(t)$ about $\tau = 2$ are functions of τ, $\vec{r}_2$, and $\dot{\vec{r}}_2$. Using the estimates of $\vec{r}_2$ and $\dot{\vec{r}}_2$, along with the functions f and g, we can get new values for a_1, a_3, $\vec{r}_2$, and $\dot{\vec{r}}_2$:

$$\vec{r}_2 = \frac{g_3\vec{r}_1 - g_1\vec{r}_3}{f_1 g_3 - f_3 g_1}; \dot{\vec{r}}_2 = \frac{f_3\vec{r}_1 - f_1\vec{r}_3}{f_3 g_1 - f_1 g_3} \tag{12}$$

$$a_1 = \frac{g_3}{f_1 g_3 - f_3 g_1}; a_3 = \frac{-g_1}{f_1 g_3 - f_3 g_1} \tag{13}$$

With these equations, the iteration can truly begin. There are five basic steps to *The Iteration*:

1) Given a_1 and a_3, use equation (7) to get new ρ_1, ρ_2, and ρ_3 values
2) We then use ρ_1, ρ_2, and ρ_3 and equations (8)-(10) to get new $\vec{r}_1$, $\vec{r}_2$, and $\vec{r}_3$ values.
3) Then use $\vec{r}_1$, $\vec{r}_2$, and $\vec{r}_3$ and the two equations in (12) to get a new $\dot{\vec{r}}_2$ value (and perhaps a new $\vec{r}_2$ value).
4) Then use $\dot{\vec{r}}_2$ and $\vec{r}_2$ and the equations in (13) to get new a_1 and a_3 values.
5) Finally, go back to 1. and repeat.

VI. Classical Orbital Elements

After the equatorial vectors were determined through the method of Gauss, they were rotated to the ecliptic plane through a rotation by $-\epsilon$ along the x-axis. From there, the classical orbital elements can be found. The six classic orbital elements characterize the asteroid's path of motion. They can be categorized in the following groups based on what orbital characteristic each orbital element determines.

Size and shape:

The asteroid's orbit is elliptical in shape with the Sun at one focus.

Semi-major axis (*a*)-

The semi-major axis is the ellipse's longest radius. This value, *a*, measures the size of the asteroid orbit. The semi-major axis can be found using the Vis-Viva Equation:

$$a = \frac{1}{\left[\frac{2}{|\vec{r}|} - \frac{|\dot{\vec{r}}|^2}{\mu}\right]} \tag{14}$$

Eccentricity (*e*)-

The eccentricity of an ellipse is the ratio between the center-to-focus distance and the semi-major axis. The value, *e*, measures how much the ellipse deviates from a circle. The eccentricity is found by using the angular momentum, velocity, and radial vectors, which always points towards the perihelion; expressed in terms of $\vec{r}$ and $\dot{\vec{r}}$:

$$e = \sqrt{1 - \frac{|\vec{r} \times \dot{\vec{r}}|^2}{\mu a}} \tag{15}$$

Orientation:

Inclination (*i*)-

The inclination is an angle that describes the tilt of the orbital plane compared to the ecliptic plane. Inclination, *i*, can be calculated using:

$$i = \cos^{-1}\left[\frac{(\vec{r} \times \dot{\vec{r}})_z}{|\vec{r} \times \dot{\vec{r}}|}\right] \tag{16}$$

Longitude of the Ascending Node (Ω)-

The longitude of the ascending node is the angle between the vernal equinox and the ascending node. The angle, Ω, can be calculated by solving for Ω in the following two equations:

$$\sin\Omega = \frac{h_x}{h \sin i} \tag{17}$$

$$\cos\Omega = -\frac{h_y}{h \sin i} \tag{18}$$

Argument of Perihelion (ω)-

The argument of perihelion is defined as the angle between the ascending node and the perihelion (the point in the orbit where the object is closest to the sun). The full derivation of ω is not included but essentially the argument of perihelion can be caluculated using the following:

$$\omega = U - v \tag{19}$$

where *U* is the distance (in radians) the asteroid traveled along its orbit since crossing the ascending node and *v* is the true anomaly, or the angle between the perihelion and the current position.

Position within orbit:

Mean Anomaly (*M*)-

The mean anomaly, *M*, represents asteroidâĂŹs position based on the area swept out in the elliptical orbit within a given time. The value of the mean anomaly "angle" is determined through the use of the eccentric anomaly, *E*. The following equation relates the two values:

$$M = E - e \sin E \tag{20}$$

After correcting for the time difference between the time of observation and ephemeris date, the resulting angle is the

mean anomaly value obtained at the time of the middle observation.

VII. Orbit Simulation

A visual simulation of the orbit of 1685 Toro, with repsect to Earth and the Sun, was created in visual python. The bodies' positions were calculated continuously using the classical Runge-Kutta method of numerical integration and then displayed in VPython.

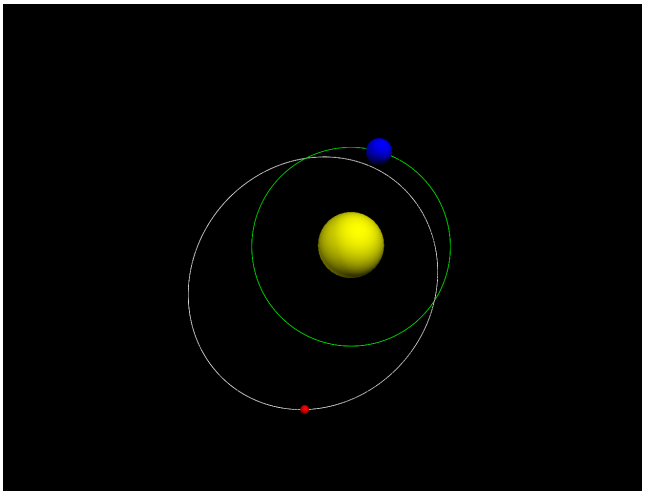

Fig. 2: *Top-down view of the VPython simulation showing 1685 Toro's orbit.*

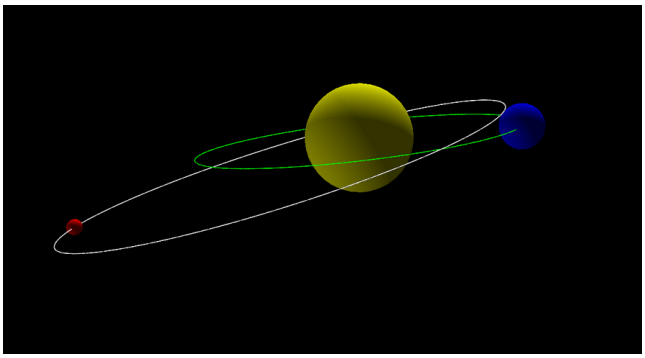

Fig. 3: *Side view of the VPython simulation showing 1685 Toro's orbit.*

VIII. Problems in Observation

While taking images with the telescope at Etscorn observatory, we encountered frequent issues with the weather at the scheduled times of observation. This was unavoidable and unfortunate, as late June and July is monsoon season in New Mexico. During some cancelled observations, we had requested data from Skynet in Chile, but the weather there had also prevented data collection. Other than the weather, we did not encounter any problems while observing.

III. Data and Analysis

I. Image #1 Measurement Results

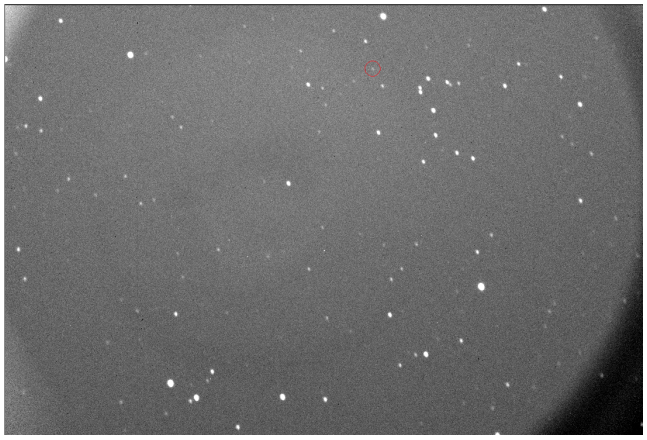

Fig. 4: *Reduced and Aligned Image of Observation #1 at Etscorn on July 2, 2015 at 04:23:44 UTC (JD: 2457205.683148148).*

Centroid Values and Uncertainties:
$\sigma_\alpha = 6.3913° \times 10^{-3}, \sigma_\delta = 6.4020° \times 10^{-3}$
$c_x = 628.013, c_y = 109.993$

Visual Magnitude:
Aperture radius: 1.5 pixels
Annulus radius (outer radius - inner radius): 4 pixels
Calculated magnitude = 15.7 V
Accepted value from JPL horizons: 15.77 V

Signal-to-Noise Ratio (SNR):
SNR = 5.92481394865

Observation #1 Values of $(\alpha_1, \delta_1, t_1)$
$\alpha_1 = 15h43m37.65s$
$\delta_1 = -24°03'30.5"$
$t_1 = 2457205.683148148$

II. Image #2 Measurement Results

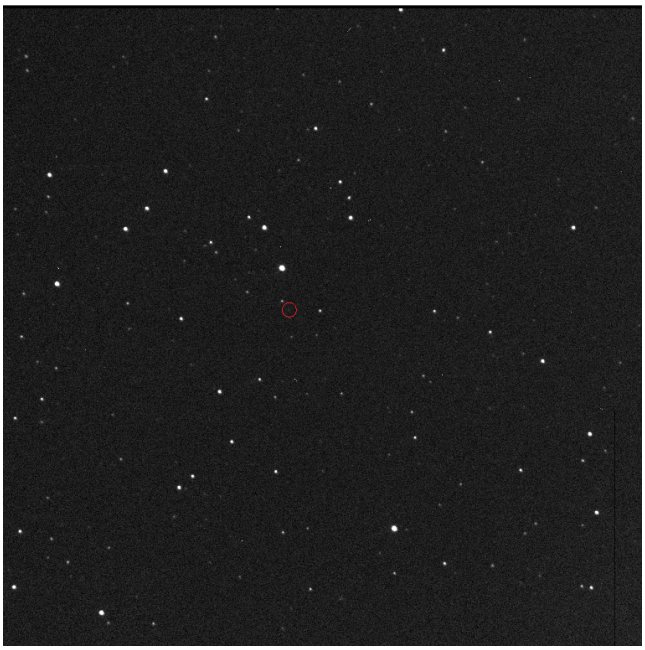

Fig. 5: *Reduced and Aligned Image of Observation #2 at Purdue on July 15, 2015 at 02:45:18 UTC (JD: 2457218.6147916666).*

Centroid values and uncertainties:
$\sigma_\alpha = 2.6217° \times 10^{-2}, \sigma_\delta = 2.6187° \times 10^{-2}$
$c_x = 1364.07, c_y = 1453.93$

Visual Magnitude:
Aperture radius: 1.5 pixels
Annulus radius (outer radius - inner radius): 5 pixels
Calculated magnitude = 15.2 V
Accepted value from JPL horizons: 16.05 V

Signal-to-Noise Ratio (SNR):
SNR = 1.43005124977

Observation #2 Values of $(\alpha_2, \delta_2, t_2)$
$\alpha_2 = 15h30m28.43s$
$\delta_2 = -21°13'04.1"$
$t_2 = 2457218.6147916666$

III. Image #3 Measurement Results

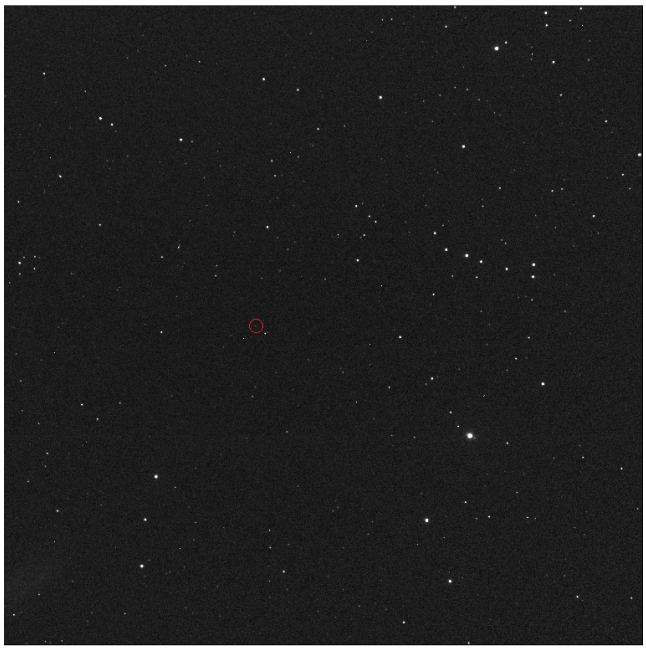

Fig. 6: *Reduced and Aligned Image of Observation #3 at Purdue on July 20, 2015 at 03:01:20 UTC (JD: 2457223.625925926).*

Centroid values and uncertainties:
$\sigma_\alpha = 2.6217° \times 10^{-2}, \sigma_\delta = 2.6187° \times 10^{-2}$
$c_x = 1364.07, c_y = 1453.93$

Visual Magnitude:
Aperture radius: 1.5 pixels
Annulus radius (outer radius - inner radius): 5 pixels
Calculated magnitude = 17.1 V
Accepted value from JPL horizons: 16.15 V

Signal-to-Noise Ratio (SNR):
SNR = 7.16274061728

Observation #3 Values of $(\alpha_3, \delta_3, t_3)$
$\alpha_3 = 15h28m11.36s$
$\delta_3 = -20°18'15.8"$
$t_3 = 2457223.625925926$

IV. Image #4 Measurement Results

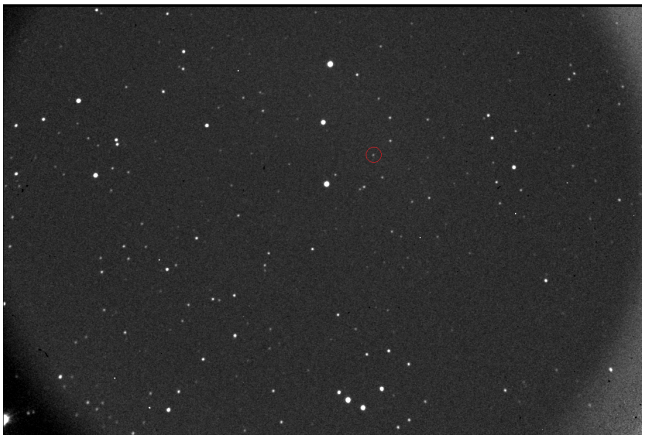

Fig. 7: *Reduced and Aligned Image of Observation #4 at Etscorn on July 21, 2015 at 04:21:40 UTC (JD: 2457224.681712963).*

Centroid values and uncertainties:
$\sigma_\alpha = 1.5027° \times 10^{-2}, \sigma_\delta = 1.4890° \times 10^{-2}$
$c_x = 631.938, c_y = 256.001$

Visual Magnitude:
Aperture radius: 1.5 pixels
Annulus radius (outer radius - inner radius): 4 pixels
Calculated magnitude = 16.0 V
Accepted value from JPL horizons: 16.16 V

Signal-to-Noise Ratio (SNR):
SNR = 4.38317554286

Observation #4 Values of $(\alpha_4, \delta_4, t_4)$
$\alpha_4 = 15h27m53.96s$
$\delta_4 = -20°07'36.9"$
$t_4 = 2457224.681712963$

V. Raw Data Processing

As previously outlined under Image Processing and Image Measuring, the raw data taken at both Etscorn and Calumet observatories had to be transformed and processed to use in the orbit determination process.

The first step in the transformation of our raw data was to identify the asteroid. Each set of raw images was reduced and combined using bias, dark, and flat frames in CCDSoft. The reduced images were then "blinked", or viewed in rapid succession. An object that moved noticeably compared to the stars around it was identified as the asteroid.

The second step was to perform astrometry through least squares plate reduction, or LSPR. Right ascensions and declinations of 24 known stars, obtained through TheSkyX, were put in a reference file along with their pixel coordinates. The reference file was processed using Python programs to produce six plate constants. The plate constants allow an object's right ascension and declination to be calculated, given its pixel coordinates.

The third step was to perform aperture photometry. A reference file was created with the pixel coordinates and magnitudes of 5 known stars, obtained through TheSkyX. By slicing out a circular aperture and background annulus around the stars, a constant was calculated. The same aperture and annulus was then applied to the asteroid. With the calculated constant, the magnitude of the asteroid could be determined. The circular aperture could also be applied in calculating signal-to-noise ratio.
The calculation of the signal-to-noise ratio (SNR) was performed using the following equation:

$$SNR = \frac{\sqrt{\dot{s}}\sqrt{t}}{\sqrt{1 + n_a p(1 + \frac{n_a p}{n_a n})\frac{(\overline{sky} + D_e + \rho^2)}{\dot{s}t}}} \tag{21}$$

The validity of the raw data was assessed by using the Image Link took in TheSkyX to link the stars in our raw images to those in the SkyX database based on the time each image was taken. All images matched the stars in the on-line database accordingly.

VI. Orbital Element Results

Each team member wrote different Orbital Determination programs, which in turn will inherently result in different values for each orbital element. Each member also accounted for uncertainty using the Jakcknife method, outlined later. Each member used the observing data from Observations 1, 2, and 4. The results are as follows:

Sean Jung's Orbital Element Results
Semimajor Axis (a): 1.38971 ± 0.00758 AU
Long. of Ascending Node (Ω): $246.3592 \pm 0.09204°$
Eccentricity (e): 0.43609 ± 0.00103
Argument of Perihelion (ω): $125.19305 \pm 0.87998°$
Inclination (i): $9.22816 \pm 0.06159°$
Mean Anomaly (M_0): $142.935997596 \pm 2.30789°$

Tiffany Pan's Orbital Element Results
Semimajor Axis (a): 1.34644 ± 0.83965 AU
Long. of Ascending Node (Ω):
$273.93700 \pm 168.60755°$
Eccentricity (e): 0.42825 ± 0.26886
Argument of Perihelion (ω): $129.39563 \pm 78.27433°$
Inclination (i): $9.37954 \pm 5.70212°$
Mean Anomaly (M_0): $130.59612 \pm 84.86667°$

Crystal Luo's Orbital Element Results
Semimajor Axis (a): 1.37446 ± 0.01112 AU
Long. of Ascending Node (Ω):
$274.05515 \pm 0.00405°$
Eccentricity (e): 0.43474 ± 0.000337
Argument of Perihelion (ω): $126.49767 \pm 0.09699°$
Inclination (i): $9.29117 \pm 0.00188°$
Mean Anomaly (M_0): $139.55928 \pm 0.85568°$

Team 4 Values
$a = 1.36717$ AU, $\Omega = 274.30235°$,
$e = .43591$, $\omega = 127.11840°$,
$i = 9.38110°$, $M_0 = 137.56764°$.

Accepted Element Values (JPL)
$a = 1.367 \pm 0.00146$ AU, $\Omega = 273.9 \pm 0.26775°$,
$e = 0.4369 \pm 0.00099$, $\omega = 127.636 \pm 0.00190°$,
$i = 9.417 \pm 0.00281°$, $M_0 = 137. \pm 0.53221°$.

VII. Classification

Based on the determined orbital elements, 1685 Toro can be classified dynamically(from the size/shape of orbit) into one of four asteroid families: Amors, Apollos, Atens, and Atiras.

The classification of asteroids into each family depends upon the semi-major axis of its orbit and the asteroid's radius at perihelion. 1685 Toro is an Apollo asteroid as its right ascension is greater than 1 AU, its r_{min} is less than 1.017, and its orbit crosses that of Earth(as shown in Figures 2 and 3). In fact, Toro has a value of r_{min} just above the 0.05 AU requirement for potentially hazardous asteroids.

IV. Conclusions

I. Results of Orbital Determination

The orbital determination revealed that Toro has a semi-major axis of approximately 1.3702 AU, an eccentricity of 0.4330, and an inclination of 9.2996°. The longitude of the ascending node is 264.7838°, the argument of the perihelion is 127.0288°, and the mean anomaly is 137.6971°.

II. Uncertainties

The experimental semi-major axis, eccentricity, inclination, and longitude of ascending node were all extremely close to the accepted JPL Horizons values, except the mean anomaly. However, the mean anomaly was still within approximately 4% of the accepted value, and is thus acceptable. Our values also greatly differed with those of Team 4, who had also observed 1685 Toro.

Uncertainties in our measurements could have resulted from human error, poor telescope calibration, or inaccurate centroids taken from unfocused images. Furthermore, some of our images had some noise due to clouds, which the data of Team 4 did not have. Also, the fact that our team observed from two different locations introduces more opportunities for error. The inferior quality of images and the extra calculations for the two different observing sites could account for the difference between our experimental values and those of Team 4 and the given JPL information. Weather and the inherent inaccuracies in changing between locations are unavoidable errors, while precision, telescope calibration, and better Python codes can be controlled to procure better results in the future.

III. Future Research

Based on the uncertainty values for our orbital elements, we have high confidence in our results. However, there is still error. One possible source of this error is the accuracy of our LSPR. Compared to the JPL Horizons ephemeris, our coordinates were slightly off. This error can accumulate with successive observations. Another source of error is our use of different observing locations. To obtain enough data for orbital determination, we took images from both Etscorn and Calumet, but the asteroid is close enough to Earth that

the coordinates change with the observing location. Taking data from both locations therefore introduced error. If one would like to replicate this experiment, one should consider taking more data points to limit the uncertainty and error.

V. Acknowledgements

The authors would like to thank Adam W. Rengstorf and Bill L. Andersen for providing guidance during the research process discussed in this paper, Devin Whitten, Linda Xu, Mathis Habich, and Elaine Johnson for their assistance and advice, Abhishek Anand for the coding help, Sukrit Tripathi, Devin Srivistava, and Elina Sendonaris for the observations they contributed, New Mexico Tech for providing us with the C-14 Telescope and a location to conduct our research, and the Summer Science Program for providing the resources and bringing this team together.

VI. Appendix

MPC Report and Cloudy Night Experiment are attached.